Neutron yields and angular distributions produced in antiproton annihilation at rest in uranium

B. Chen, T. A. Armstrong, R. A. Lewis, R. Newton, and G. A. Smith
Laboratory for Elementary Particle Science, Department of Physics, The Pennsylvania State University, University Park, Pennsylvania 16802

J. P. Bocquet and F. Malek
Institut des Sciences Nucléaires de Grenoble, 53 Avenue des Martyrs, 38026 Grenoble CEDEX, France

H. Nifenecker
Institut des Sciences Nucleaires de Grenoble CEDEX, 53 Avenue des Martyrs, 38026 Grenoble CEDEX, France and DRFMC/LIH Centre d'Etudes Nucléaires de Grenoble, Boîte Postale 85X, 38041 Grenoble CEDEX, France

M. Maurel, E. Monnand, P. Perrin, and C. Ristori
DRFMC, Centre d'Etudes Nucléaires de Grenoble, Boîte Postale 85X, 38041 Grenoble CEDEX, France

G. Ericsson, T. Johansson, and G. Tibell
Department of Radiation Sciences, P.O. Box 535, S-75121 Uppsala, Sweden

M. Rey-Campagnolle
Centre de Spectrométrie Nucléaire et de Spectrométrie de Masse, Institut National de Physique Nucléaire et de Physique des Particules, Centre National de la Recherche Scientifique F-91405 Orsay, France and CERN/PPE, CH-1211 Geneva 23, Switzerland

S. Polikanov
Gesellschaft für Schwerionenforschung Darmstadt, Postfach 110541, D-6100 Darmstadt, Germany

T. Krogulski
Warsaw University, Bialystok Branch, PL-15-424 Bialystok, Poland

J. Mougey
Continuous Electron Beam Accelerator Facility, Newport News, Virginia 23606

(Received 18 December 1991)

Measurements of neutron yields and their angular distributions in coincidence with fission fragments produced in antiproton annihilation at rest in a natural uranium target have been carried out Low Energy Antiproton Ring (LEAR) at CERN. A total of 16.3 ± 0.9 neutrons per annihilation have been found, distributed among direct knockout (27%), evaporation (21%), and fission (52%) processes. Angular distributions show that neutrons below approximately 5 MeV result entirely from moving fission fragments, and above approximately 12 MeV entirely from the excited, prescission nucleus. An estimate of the angular momentum of the excited fission fragment gives $\sim 13\hbar$. We are able to account for all baryons produced in annihilation, including neutrons from this experiment and light charged nuclei found in another LEAR experiment, to within 4.5 ± 2.5 of the initial 237 units in the initial state.

PACS number(s): 25.43.+t

I. INTRODUCTION

When an antiproton stops in uranium, it forms an antiprotonic atom which cascades down to the $n=11$, $l=10$ atomic level before annihilating [1]. The annihilation occurs on the nuclear surface, creating approximately five high-momentum pions. Typically, 30% of the pions pass through greater than one mean free path of nuclear matter, initiating an intranuclear cascade (INC). The nuclear excitation is different from that induced by particle beams in that the primary particles are born on the nuclear surface. From measurements of interactions with neutrons [2], pions [3,4], gamma rays [5], and protons [6], general properties of the INC have been characterized. However, these characterizations have little application to antiprotons, which release an extraordinarily large amount of energy into the nucleus via the annihilation process.

One of the unique features of interactions with uranium is fission. Because of the large excitation of the parent nucleus and fission fragments expected from antiproton annihilation, the study of neutron emission appears especially attractive. Results on neutron yields and decay angular distributions should offer clues to the degree of excitation of the nucleus and fragments. Previous studies from this and an earlier experiment have resulted

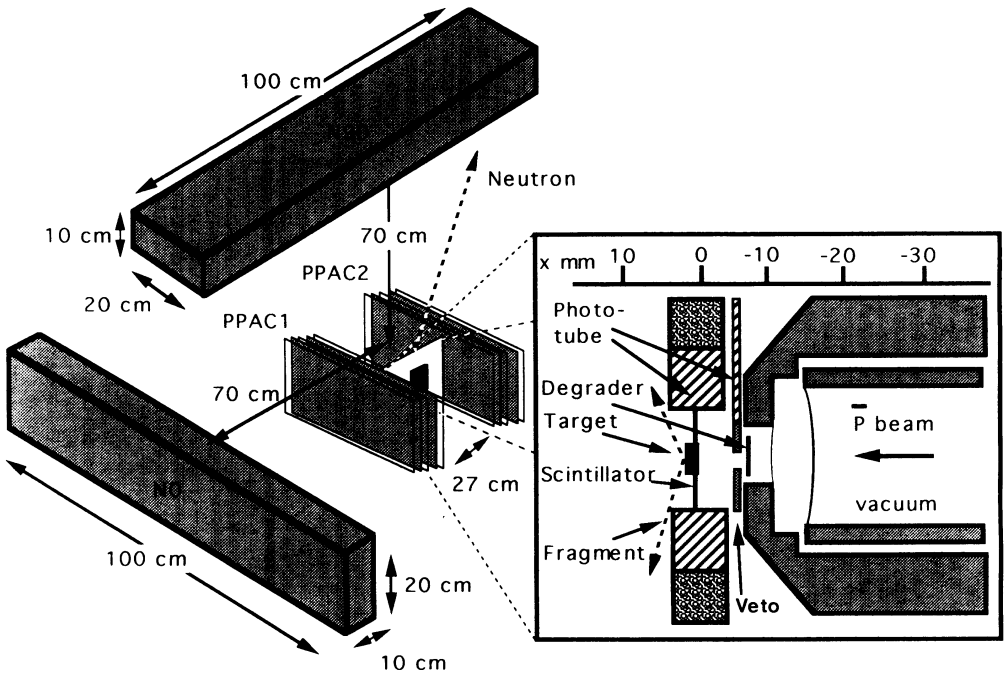

FIG. 1. Schematic layout of target, PPAC, and neutron detectors.

in the first observation of fission neutrons [7] and gamma rays [8], and a detailed measurement of the energy transfer in the INC as deduced from π^0 [9] and charged pion [10] spectra. The goal of this paper is to develop a coherent picture of antiproton-induced fission involving neutron emission, wherein yields and angular distributions are analyzed and discussed.

II. EXPERIMENT

The apparatus is shown schematically in Fig. 1. An antiproton beam with an intensity of 10^5 sec^{-1} and an initial momentum of 105 MeV/c was degraded to rest. About 2% of the antiprotons stopped in a 200-μg/cm^2 natural uranium film deposited on a 200-μm-thick scintillator. Photomultipliers provided a signal for the arrival time of each antiproton. Two parallel-plate avalanche chambers (PPAC 1,2) measured the direction of fission fragments emerging from the target. The target and PPAC's were enclosed in a vacuum box (not shown). In this analysis, valid hits in all four PPAC planes define an event in which a fission occurred. Further details of the apparatus may be found in Ref. [11].

A pair of neutron counters, $N\emptyset$ and $N9\emptyset$, were located outside the vacuum box, each at a distance of 70 cm from the target. A set of 0.6-cm-thick scintillation veto counters (not shown) placed immediately in front of the neutron counters recorded the presence of charged particles. Pulses in the neutron counters, recorded more than 2 nsec later than prompt pions with no corresponding hits in the veto counters, were identified as neutrons. The neutron detectors are described in further detail in Ref. [7].

III. NEUTRON YIELDS

Figure 2 shows the neutron momentum spectrum deduced from hits in the neutron counters. Numerical values for the data are listed in Table I. The distribution has been corrected for (a) solid angle, (b) counting efficiency, (c) background from secondary interactions, and (d) electronic pileup. Solid-angle and counting efficiency corrections were determined using a Monte Carlo simulation. Neutrons from the uranium target were projected toward the neutron counters. The pulse height resulting from an interaction in the counters was calculated using the techniques of Cecil *et al.* [12], converting energy deposition into equivalent electron energy.

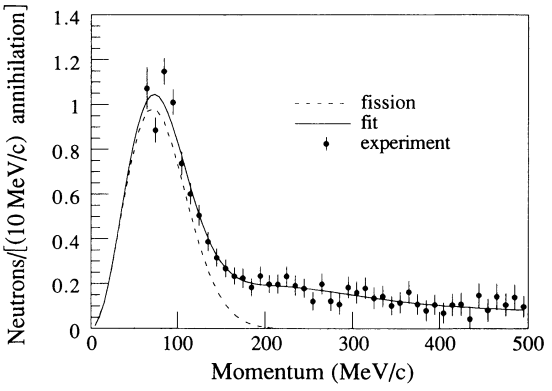

FIG. 2. Measured neutron momentum distribution. The solid line is a three-component fit to the data. The dashed line is the fission component. See text for details.

The cutoff energies for the counters, 0.46±0.02 MeV for $N\emptyset$ and 0.36±0.02 MeV for $N9\emptyset$, were determined by adjusting the simulated spectra to agree with the data for momenta of 50–80 MeV/c.

Background from secondary interactions was measured in runs using a target consisting of a scintillator with no uranium coating. The requirement for fission fragment hits in the PPAC's was removed for these runs. Background subtractions were typically 20% of the data taken with the uranium coating. No hits were observed in $N\emptyset$ or $N9\emptyset$ in 68% of the events. In the remaining events, hits were observed mostly (~90%) due to prompt pions and gamma rays. Since the time-to-digital converters recorded only the first of multiple hits, the neutron yields shown in Fig. 2 have been multiplied by 1/0.68 to correct for pileup effects.

TABLE I. Experimental data (Fig. 2). Units are number of neutrons per 10 MeV/c per annihilation.

Momentum	Data	±error
65	1.0719	0.0924
75	0.8862	0.0547
85	1.1477	0.0586
95	1.0103	0.0556
105	0.7377	0.0506
115	0.6018	0.0475
125	0.5058	0.0463
135	0.3885	0.0430
145	0.3164	0.0405
155	0.2681	0.0395
165	0.2338	0.0385
175	0.2253	0.0434
185	0.1835	0.0389
195	0.2345	0.0416
205	0.1980	0.0396
215	0.1971	0.0436
225	0.2331	0.0437
235	0.1920	0.0456
245	0.1795	0.0426
255	0.1221	0.0413
265	0.1989	0.0462
275	0.1230	0.0435
285	0.1087	0.0458
295	0.1838	0.0482
305	0.1610	0.0492
315	0.1804	0.0482
325	0.1357	0.0482
335	0.1436	0.0483
345	0.1025	0.0421
355	0.1157	0.0474
365	0.1631	0.0498
375	0.1090	0.0459
385	0.0803	0.0470
395	0.1070	0.0446
405	0.0703	0.0462
415	0.1059	0.0495
425	0.1088	0.0510
435	0.0438	0.0500
445	0.1485	0.0533
455	0.0823	0.0504
465	0.1423	0.0581
475	0.1059	0.0503
485	0.1398	0.0556
495	0.0984	0.0479

The neutron spectrum is expected to be composed of high-momentum neutrons from direct knockout INC processes, and low-momentum neutrons from evaporation and fission [7]. The fit (solid curve) in Fig. 2 is the sum of three components: fission (post-scission), evaporation (pre-scission), and direct (pre-scission) neutrons:

$$\frac{dN}{dp} = a_F\beta\frac{e^{-E_F/T_F}}{(\pi E_F T_F)^{1/2}}\sinh(2\sqrt{E_F E}\,/T_F)e^{-E/T_F} \quad \text{(fission)} \quad (1)$$

$$+a_{\mathrm{EV}}\beta\frac{2\sqrt{E}\,e^{-E/T_{\mathrm{EV}}}}{\sqrt{\pi}T_{\mathrm{EV}}^{3/2}} \quad \text{(evaporation)} \quad (2)$$

$$+a_D\beta\frac{2\sqrt{E}\,e^{-E/T_D}}{\sqrt{\pi}T_D^{-3/2}} \quad \text{(direct)}\,, \quad (3)$$

where E is the neutron kinetic energy, β is the neutron velocity divided by the speed of light, E_F is the mean fission fragment kinetic energy per u, and T_F, T_{EV}, and T_D are the temperatures of neutrons from the fission, evaporation, and direct processes, respectively. Equation (1) follows from the model of Watt [13]. The yield and temperature parameters found by fitting to the sum of Eqs. (1)–(3) are given in Table II. Yields are integrated so that the factors a_F, a_{EV}, and a_D refer to the number of neutrons per annihilation, from 0 to 1000-MeV/c momentum.

The average atomic number of the fragments from this experiment is $A=106\pm1$ [14]. Therefore, the fragment energy per u (E_F) of 0.74±0.12 MeV corresponds to a kinetic energy of 79±13 MeV, or 158±26 MeV for the sum of the two fragment kinetic energies. This value is in good agreement with the measurement of Bocquet *et al.* [14], where the fission fragment energy was determined directly. A Fermi-gas model of the excited fission fragments relates the excitation energy, E_F^*, to the fragment temperature as [15]

$$E_F^* = aT_F^2 = 51\pm10 \text{ MeV}\,, \quad (4)$$

where the level density parameter $a=A/(10\pm1)=10.6\pm1.1$ MeV^{-1}. Summing over the two fragments gives 102±20 MeV, which is 22±5% of the 455±50 MeV previously determined to be transferred to

TABLE II. Fitted neutron yield and temperature parameters. See text for details.

a_D (no./ann)	4.49±0.75
T_D (MeV)	99.6±11.1
a_{EV} (no./ann)	3.40±0.35
T_{EV} (MeV)	18.9±2.0
a_F (no./ann)	8.42±0.25
T_F (MeV)	2.18±0.20
E_F (MeV/nucleon)	0.74±0.12
Total no. neutrons	16.3±0.9

the nucleus from the initial antiproton annihilation [10].

The portion of the fragment excitation energy, which is in the form of fission neutron kinetic energy (dashed curve, Fig. 2), is

$$E_K = (8.42 \pm 0.25) \times \tfrac{3}{2}(2.18 \pm 0.20) = 28 \pm 3 \text{ MeV} .$$

In addition, nuclear gamma rays account for energy $E_\gamma = 12 \pm 2$ MeV [8]. Therefore, assuming ~6-MeV binding energy for each of the neutrons released, ~88% of the fragment excitation energy is attributed to neutron and gamma-ray emission.

For comparison, the values of these parameters for low-energy neutron-induced fission of uranium are approximately $E_F^* = 21$ MeV [using a temperature of 1.4 MeV in Eq. (4)], $E_K = 5.3$ MeV neutron kinetic energy and $E_\gamma = 10.7$ MeV gamma-ray energy [2,16]. Including ~6 MeV binding energy for each of the 2.5 neutrons released, the corresponding fraction of neutron and gamma-ray energy of the total excitation energy is 74%, somewhat smaller than the value for antiproton-induced fission.

IV. NEUTRON ANGULAR DISTRIBUTIONS

The angular distribution of the neutrons with respect to the fragment direction is related to their angular momentum, and to whether they are emitted before or after scission.

Figure 3 shows the laboratory angular distribution between the neutron and fission fragment detected in PPAC-1, for momenta of (a) 60–100 MeV/c and (b) 100–150 MeV/c. Since the apparatus cannot distinguish which fragment emitted the neutron, all spectra are measured with respect to PPAC-1. Geometrical, electronic, and background corrections have been applied on a bin-by-bin basis. The simulation includes a 10-cm rms smearing to account for the spatial resolution of the neutron detectors. The data have been fit (solid line) by a function consisting of three terms, representing decays which are (a) isotropic in the laboratory, allowing for neutrons coming directly from the decay of the parent nucleus before scission, (b) isotropic in the fission fragment rest frame, and (c) characterized by a $\cos^2(\theta)$ distribution in the fission fragment rest frame. Due to Lorentz effects, terms (b) and (c) both contribute to nonisotropy in the laboratory frame. The dashed line in Fig. 3 shows the contribution of term (a), which is large (77% of integrated yield) above 100 MeV/c.

The results may be understood by looking at various ratios, such as the fission fraction

$$\text{FF} = (b + c)/(a + b + c) , \tag{5}$$

which should be equal to unity if all neutrons emerge after scission. In Table III we show this ratio, which is also plotted in Fig. 4 (open circles), as a function of the neutron momentum. Also shown in Fig. 4 are the results of fits to the momentum spectrum (solid circles) discussed previously. We see that, for momenta below 100 MeV/c, both sets of data are consistent with 100% post-scission neutron emission. However, in the interval 100–150 MeV/c, there is clear evidence for pre-scission neutrons.

TABLE III. Parameters resulting from fits to neutron angular distribution versus neutron momentum. See text for details.

Momentum (MeV/c)	FF	A	χ^2/deg freedom
60–80	1.060±0.165	0.171±0.081	0.69
80–100	0.800±0.125	0.287±0.132	1.12
100–150	0.232±0.092	0.571±0.776	0.88
150–200	−0.044±0.127		0.54
200–300	0.072±0.070		1.05
300–500	−0.036±0.089		0.80

The spectrum is completely dominated by pre-scission neutrons above approximately 150 MeV/c (12-MeV kinetic energy). A measurement with 155-MeV protons [6] gives a ratio of post-scission to pre-scission neutrons of 0.88±0.05 for neutrons up to 9-MeV kinetic energy. We find a slightly larger value of 1.08±0.29 for the same neutron energy interval.

In Table III we also show values of the anisotropy

$$A = c/b \tag{6}$$

for the 0–150-MeV/c interval where the data result pri-

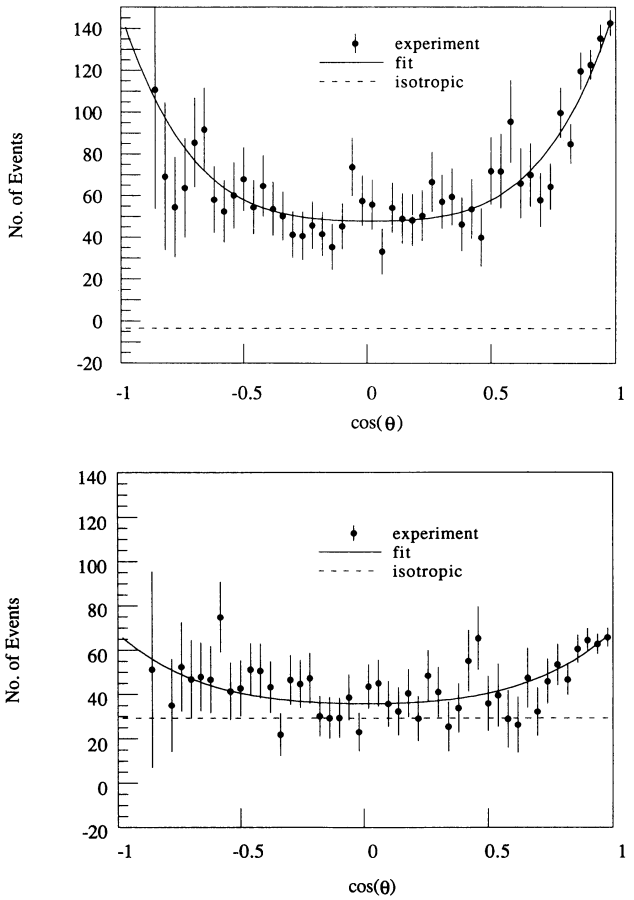

FIG. 3. Neutron laboratory angular distribution for neutron momenta in the range (a) 60–100 and (b) 100–150 MeV/c. The solid lines are fits to the data. The dashed curve is the isotropic part of the fit. See text for details.

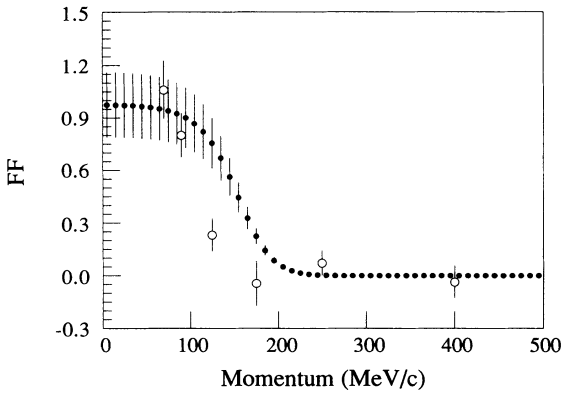

FIG. 4. Fraction of events attributed to fission vs neutron momentum. The (open) solid points are the fraction based on fits to (angular) momentum distributions.

marily from fission. The anisotropies found in our data are substantially larger than those observed (10–15 %) in spontaneous fission of ^{252}Cf [15]. A measurement of 155 MeV protons [6], where one expects large energy transfer to the nucleus, finds no significant anisotropy of neutrons in the fragment rest frame. This is consistent, as will be shown, with a model in which substantial angular momentum is transferred to the fragment in antiproton-induced fission.

The anisotropy may also be used to deduce the moment of inertia of the decaying fission fragment. Following the analysis of Gavron [17] on angular distributions of neutrons from fission fragments, the anisotropy depends on the dimensionless quantity $B^2=2IT/\hbar^2$, where I is the moment of inertia of the nucleus and T is its temperature. By linear extrapolation of Gavron's analysis from values of $(B, A)=(6,0.075)$ and (11,0.15), we estimate that $B\simeq 15$ for $A=0.22\pm0.08$ (average of first two entries of Table III). Using $T=2.18$ MeV from Table II, it follows that $2I/\hbar^2$ is approximately 103 MeV^{-1}. This value is comparable to the value of 86 MeV^{-1} from Gavron's analysis, assuming $B=11$ and $T=1.4$ MeV, which is characteristic of fission fragments due to low-energy neutron-induced or spontaneous fission. For additional comparison, we find that the moment of inertia of a rigid sphere, given by $I=2/5AR^2$ with $A=106$ and $R=1.3A^{1/3}$ fm, leads to a value of $2I/\hbar^2=78$ MeV^{-1}. These comparisons suggest that the difference in anisotropies between antiproton-induced fission and low-energy neutron-induced or spontaneous fission is more related to temperature than to moment of inertia.

Knowledge of the B parameter allows one to estimate the angular momentum of the decaying fission fragment. One may assume that the initial spin distribution is of the form [17]

$$P(J)=(2J+1)\exp[-J(+\tfrac{1}{2})^2/B^2]\ . \quad (7)$$

By integrating over this distribution, we find that the average angular momentum for $B=15$ is $\bar{J}=13\hbar$. By comparison, we note that the average angular momentum of fission fragments produced in low-energy neutron-induced or spontaneous fission is in the range $(4-8)\hbar$ [18]. In the classical approximation each neutron of average momentum 80 MeV/c emitted from a nucleus of radius 6.2 fm carries away approximately $2.5\hbar$ of angular momentum. Therefore, it is quite plausible that an excited nucleus with $J=13\hbar$ could decay sequentially on average into 4.2 neutrons ($a_F/2$, see Table II) plus 2.0 gamma rays [8].

V. DISCUSSION

A previous measurement of neutrons from antiproton annihilation at rest in uranium [7] was made, using high-momentum pions and protons in a spectrometer as a trigger, and a neutron counter array 180° opposite to the spectrometer. This measurement reported 5.77 ± 0.16 neutrons/annihilation, less than half the 16.3 ± 0.9 neutrons per annihilation given in Table II. This effect may be qualitatively explained from energy considerations. Because the trigger particle carries away a large energy (typically 400 MeV), in general, the fissioning nucleus, and hence fission fragments, will be in a relatively unexcited state, leading to the emission of fewer neutrons than on average.

Finally, it is of interest to account for nucleons in antiproton-induced fission of uranium. The nucleons observed in this experiment are (1) fission fragments -212 ± 2, (2) evaporation plus direct neutrons -7.9 ± 0.8, and (3) fission neutrons -8.4 ± 0.3, for a total of 228.3 ± 2 nucleons. The initial antiproton, uranium state contains 237 nucleons, leaving 8.7 ± 2.0 nucleons unaccounted for in this experiment. In another experiment, yields of low-energy light nuclei (p, d, t, He, and Li) have been measured for antiproton annihilation at rest in uranium [19,20]. The total number of nucleons reported is 4.5 ± 1.4, leaving a balance of 4.2 ± 2.5 nucleons. We ascribe this small difference to possible statistical or systematic errors in the measurements.

ACKNOWLEDGMENTS

The authors express their thanks to the builders and operators of LEAR at CERN, whose diligent and inspired efforts enabled the acquisition of the data presented in this paper. We also thank Dr. Joseph Cugnon, Dr. Peter Hofmann, and Dr. David Madland for private discussions concerning the interpretation of the data. This work was supported in part by the U.S. Air Force Office of Scientific Research under Grants Nos. 87-0246 and 91-0302.

[1] P. Jasselette, J. Cugnon, and J. Vandermeullen, Nucl. Phys. **A484**, 542 (1988).
[2] R. Vandenbosch and J. R. Huizenga, *Nuclear Fission* (Academic, New York, 1973).
[3] H. P. Isaak *et al.*, Nucl. Phys. **A392**, 368 (1983).
[4] K. H. Hicks, *et al.*, Phys. Rev. C **31**, 1323 (1985).
[5] E. J. Winhold, P. T. Demos, and I. Halpern, Phys. Rev. **87**, 1139 (1952).

[6] E. Cheifetz and Z. Fraenkel, Phys. Rev. C **2**, 256 (1970).
[7] A. Angelopoulos *et al.*, Phys. Lett. B **205**, 590 (1988).
[8] T. A. Armstrong, R. Bishop, V. Harris, R. A. Lewis, E. Minor, and G. A. Smith, Z. Phys. A **331**, 519 (1988).
[9] T. A. Armstrong, R. Bishop, V. Harris, R. A. Lewis, E. Minor, and G. A. Smith, Z. Phys. A **332**, 467 (1989).
[10] E. D. Minor, T. A. Armstrong, R. Bishop, V. Harris, R. A. Lewis, and G. A. Smith, Z. Phys. A **336**, 461 (1990).
[11] J. P. Bocquet *et al.*, Phys. Lett. B **182**, 146 (1986); J. P. Bocquet *et al.*, *ibid.* **192**, 312 (1987); M. Rey-Campagnolle, Il Nuovo Cimento **102A**, 653 (1989); S. Polikanov, Nucl. Phys. **A502**, 195c (1989).
[12] R. A. Cecil, B. D. Anderson, and R. Madey, Nucl. Instrum. Methods **161**, 439 (1979).
[13] B. E. Watt, Phys. Rev. **87**, 1037 (1952).
[14] J. P. Bocquet *et al.*, Z. Phys. A (to be published); F. Malek, Ph.D. thesis, l'Université Joseph Fourier, Grenoble, France, 1990.
[15] D. G. Madland and J. R. Nix, Nucl. Sci. Eng. **81**, 213 (1982).
[16] V. M. Gorbachev, Y. S. Zamyatnin, and A. A. Lbov, *Nuclear Reactions in Heavy Elements* (Pergamon, New York, 1980).
[17] A. Gavron, Phys. Rev. C **13**, 2562 (1976).
[18] J. B. Wilhelmy, E. Cheifetz, R. C. Jared, S. G. Thompson, and H. R. Bowman, Phys. Rev. C **5**, 2041 (1972).
[19] W. Markiel *et al.*, Nucl. Phys. **A485**, 445 (1988).
[20] P. Hofmann *et al.*, Nucl. Phys. **A572**, 669 (1990).

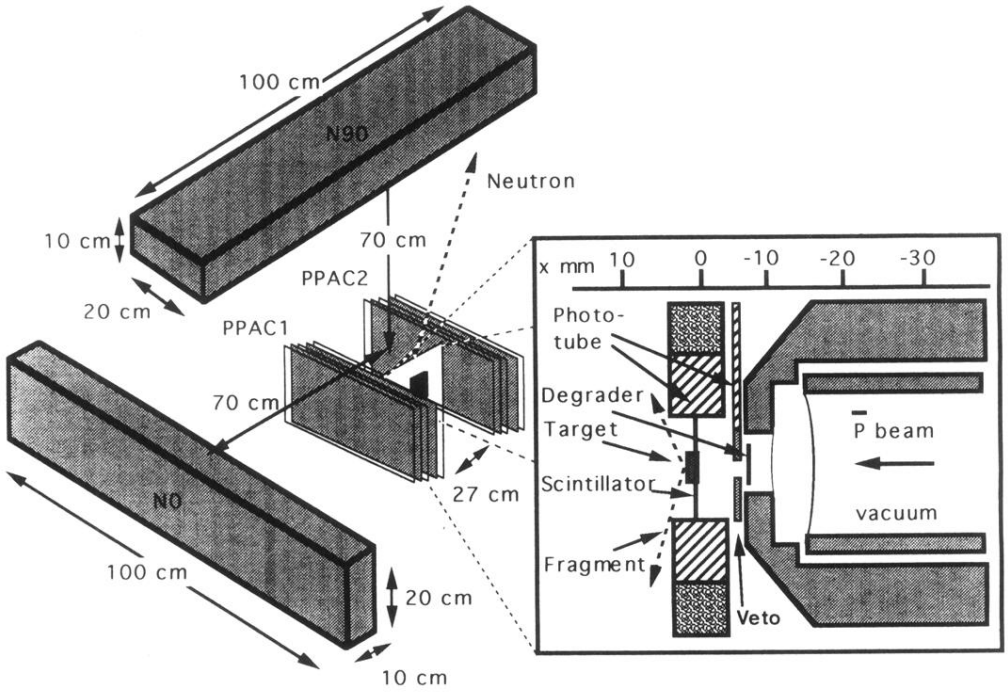

FIG. 1. Schematic layout of target, PPAC, and neutron detectors.